THE JOURNAL OF PHYSICAL CHEMISTRY B
A JOURNAL OF THE AMERICAN CHEMICAL SOCIETY

pubs.acs.org/JPCB

Article

Hydration and Seamless Integration of Hydrogen Peroxide in Water

Aria J. Bredt, Denilson Mendes de Oliveira, Andres S. Urbina, Lyudmila V. Slipchenko, and Dor Ben-Amotz*

Cite This: *J. Phys. Chem. B* 2021, 125, 6986–6993

Read Online

ACCESS | Metrics & More | Article Recommendations | Supporting Information

ABSTRACT: Raman multivariate curve resolution is used to decompose the vibrational spectra of aqueous hydrogen peroxide (H_2O_2) into pure water, dilute H_2O_2, and concentrated H_2O_2 spectral components. The dilute spectra reveal four sub-bands in the OH stretch region, assigned to the OH stretch and Fermi resonant bend overtone of H_2O_2, and two nonequivalent OH groups on water molecules that donate a hydrogen bond to H_2O_2. At high concentrations, a spectral component resembling pure H_2O_2 emerges. Our results further demonstrate that H_2O_2 perturbs the structure of water significantly less than either methanol or sodium chloride of the same concentration, as evidenced by comparing the hydration-shell spectra of *tert*-butyl alcohol dissolved in the three aqueous solutions.

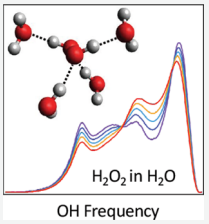

INTRODUCTION

The similar chemical structures of hydrogen peroxide (H_2O_2) and water (H_2O) suggest that their mixtures may be uniquely compatible. Previous thermodynamic,[1−4] structural,[2,5−10] spectroscopic,[4,5,7,8,11−18] and theoretical[5,18−22] studies of pure H_2O_2[5−8,11,13−15] and its aqueous mixtures[1,2,4,9,10,14,15,18−20] have revealed some striking similarities between H_2O_2 and water but have not measured the hydration-shell spectrum of dilute aqueous H_2O_2 or quantified the influence of H_2O_2 on water structure. Here, we do so by using Raman multivariate curve resolution (Raman-MCR) spectroscopy, revealing four distinct sub-bands in the OH stretch region of dilute aqueous H_2O_2, whose assignments are aided by the previously reported crystal structure[9] and the vibrational spectra[23,24] of solid $H_2O_2 \cdot 2H_2O$ as well as our own vibrational frequency calculations. Our results demonstrate the remarkable insensitivity of water structure to the addition of H_2O_2 by showing that the hydration-shell spectrum of *tert*-butyl alcohol (TBA) is far less perturbed by the addition of 5 M H_2O_2 than by either methanol (CD_3OH) or NaCl of the same concentration. Beyond the intrinsic interest of H_2O_2 as a flexible and chiral waterlike molecule, its suppression of ice nucleation[1,2] may facilitate future supercooled water studies.[25−28]

Although pure H_2O_2 and H_2O have similar freezing points[1,2] and dielectric constants,[4] their mixtures have a freezing point minimum near −50 °C, and both pure liquid H_2O_2 and aqueous H_2O_2 are more readily supercooled than pure water.[1,2] Such mixtures also have a larger dielectric constant[15] and longer relaxation times[16,17] than water, as well as a negative excess enthalpy, entropy, and Gibbs energy of mixing.[3,4] Similarities between H_2O_2 and water are apparent in the vibrational spectra of H_2O_2 in the vapor,[5,12] liquid,[11,14] and solid[13] phases, as well as solid H_2O_2 dihydrate[23,24] and liquid aqueous H_2O_2 solutions.[14,29] The experimental structure of the solid H_2O_2 dihydrate[9] as well as $(H_2O_2)_n(H_2O)_m$ cluster calculations[20−22,30,31] and liquid molecular dynamics (MD) simulations with *ab initio*,[19,20] hybrid quantum/classical,[32] and classical polarizable[21] force fields indicate that replacement of the oxygen atom in H_2O by a pair of oxygen atoms in H_2O_2 has relatively little influence on the first hydration shell of the two molecules, both of which favor hydrogen bonding to the four nearest neighbor water molecules with an approximately tetrahedral geometry.

An important difference between the structure of water and H_2O_2 results from rotations about the O−O bond axis of H_2O_2, which facilitate the adoption of a range of dihedral angles (ϕ) between the two OH groups, ranging from the limiting cis ($\phi = 0°$, C_{2v}) to trans ($\phi = 180°$, C_{2h}) structures. In both gas and solid phases, the most stable conformation of H_2O_2 has an open book ($0° < \phi < 180°$, C_2) structure but with different mean dihedral angle values in gas ($\phi \sim 114°$)[5] and anhydrous ($\phi \sim 90°$)[7] and dihydrate ($\phi \sim 130°$)[9] solids. The variation in these equilibrium dihedral angles attests to the significant flexibility of this degree of freedom, as also evidenced in $(H_2O_2)_n(H_2O)_m$ cluster calculations in which H_2O_2 is found to adopt open book conformations with a wide range of dihedral angles.[20−22,30,31]

All H_2O_2 open book structures are chiral and thus can adopt mirror image ($\pm\phi$) conformations.[21,32] Interconversion of the two enantiomers of H_2O_2 is predicted to go through a trans transition state in both the gas phase (isolated H_2O_2) and aqueous H_2O_2 solutions.[32] The rate of interconversion in the aqueous solution is predicted to be significantly longer than 50 ps.[20,32] Thus, the apparently different populations of the so-called cisoid ($0° < \phi < 180°$) and transoid ($180° < \phi < 360°$)

Received: April 9, 2021
Revised: May 19, 2021
Published: June 16, 2021

https://doi.org/10.1021/acs.jpcb.1c03107
J. Phys. Chem. B 2021, 125, 6986–6993

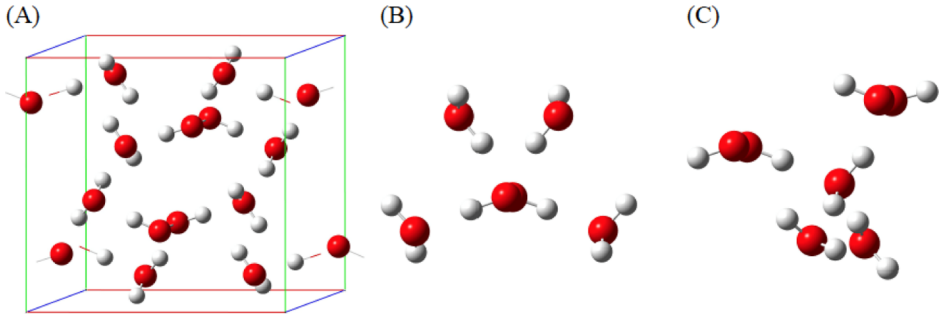

Figure 1. Structure of (A) the H_2O_2 dihydrate unit cell, (B) the $H_2O_2{\cdot}4H_2O$ cluster, and (C) the $2H_2O_2{\cdot}3H_2O$ cluster, whose oxygen atom positions are the same as those in the dihydrate crystal.

structures in aqueous H_2O_2, reported in recent *ab initio* force field simulations,[19] are evidently artifacts resulting from nonequilibration on the short (≲50 ps) simulation time scales since the equilibrium distributions with $0° < \phi < 180°$ and $180° < \phi < 360°$ must be equally populated mirror images of each other. Longer (∼5 ns) simulations of pure liquid H_2O_2, performed using classical polarizable ABEEM/MM force fields, predicted an open book conformational population that peaked near $\phi \sim 105°$ (and presumably an equally populated mirror image distribution that peaked near $\phi \sim -105° \equiv 255°$).[21] The chirality of H_2O_2 also influences its solid crystal structures as pure H_2O_2 forms two chiral crystal enantiomorphs, each of which contain only one optical isomer of H_2O_2[6−8] (as is also predicted to be the case for some gas-phase clusters of H_2O_2),[21] while the H_2O_2 dihydrate crystal has a nonchiral centrosymmetric structure in which both mirror image enantiomers occupy each unit cell.[8,9]

MATERIALS AND METHODS

Experimental Methods. Aqueous solutions were produced from deionized filtered water (18.2 MΩ cm, Milli-Q UF plus), hydrogen peroxide (Sigma-Aldrich, 30 wt %), CD_3OH (d_3-methanol, CDN isotopes, 99.9 atom % D), sodium chloride (Mallinckrodt, >99.9%), and TBA (Sigma-Aldrich, ≥99.7%). Solutions of the desired concentrations were prepared in 10 mL volumetric flasks into which the appropriate number of moles of solute(s) were transferred either by volume (30 wt % hydrogen peroxide and methanol) or by weight (TBA and NaCl) followed by the addition of enough water to produce a total volume of 10 mL. The resulting solutions were equilibrated by repeated inversion to ensure dissolution and uniform mixing before pipetting ∼2 mL into 1 cm spectroscopic glass cuvettes capped with a Teflon stopper.

Raman measurements of the solutions were performed in a temperature-controlled cell holder (Quantum Northwest)[33] equilibrated to 20.0 °C (unless stated otherwise). Raman spectra were collected as previously described[34] using a home-built Raman system with an Ar-ion laser of 514.45 nm wavelength and ∼20 mW power at the sample, a 300 mm spectrograph (SpectraPro300i, Acton Research Inc.) with a 300 grooves per mm grating, and a thermo-electrically cooled CCD camera (Pixis 400B, Princeton Instruments Inc.). The resulting spectra spanned the entire vibrational frequency range from ∼100 cm^{-1} to over ∼4000 cm^{-1} with a dispersion of ∼5.5 cm^{-1} per pixel in the OH stretch region. The ∼667.83 nm line from a neon calibration lamp with a 670 nm bandpass filter was included in each Raman spectrum and used to precisely align the wavelengths (with subpixel resolution) of all spectra collected on the same day under essentially identical conditions.[33] A constant numerical background (equal to the global minimum of the entire set of spectra) was subtracted from each spectrum prior to the self-modeling curve resolution (SMCR) analysis.

Raman-MCR Analysis Methods. Raman-MCR spectral decompositions were performed using the SMCR algorithm[35] to decompose the solution spectra into solvent and solute-correlated (SC) component spectra.[36,37] The first round of SMCR decomposition was performed using pairs of spectra, one of which was pure water and the other an aqueous solution. Decomposition of the aqueous H_2O_2 spectra was performed after smoothing the input spectra using the Savitzky−Golay algorithm[38,39] with an 11-pixel window width to reduce the noise of the low concentration SC spectra with no significant change in the shape of the SC OH stretch band shape (although the OO stretch band was slightly broadened). The small remaining background was subtracted from all SC spectra using a cubic polynomial fit to selected background pixels spanning the OO to OH spectral range. All H_2O_2 SC spectra were normalized to the same concentration by dividing by the OO band area (whose intensity is linearly correlated with concentration), and the TBA solution spectra were normalized by dividing each spectrum by the TBA CH band area.

The second-round SMCR decomposition of the first-round SC spectra of H_2O_2 was performed as follows. First, the normalized and background subtracted SC spectra with concentrations from 1 to 9.8 M were simultaneously processed using SMCR to obtain the two spectral components that best regenerate all spectra. Then, the corresponding spectral weights of the two components were plotted as a function of H_2O_2 concentration and fit to quadratic functions of the concentration. The component spectral weights were then extrapolated to zero concentration and used to reconstruct the infinitely dilute H_2O_2 SC spectrum. Subsequently, another round of SMCR decomposition was performed using the same concentration-dependent first-round SC spectra as well as the extrapolated infinitely dilute SC spectrum. Thus, each of the first-round SC spectra were decomposed into a linear combination of the infinitely dilute spectrum (isolated H_2O_2) and a new spectral component that emerges with increasing concentration, assigned to interacting H_2O_2 molecules.

Computational Methods. The crystal structure of the H_2O_2 dihydrate,[9] whose unit cell is shown in Figure 1A, is used to construct the two clusters shown in Figure 1B,C. The first of these clusters consists of a hydrogen peroxide molecule and its first coordination shell ($H_2O_2{\cdot}4H_2O$), and the second consists of the water molecule that donates a hydrogen bond to H_2O_2

https://doi.org/10.1021/acs.jpcb.1c03107
J. Phys. Chem. B 2021, 125, 6986−6993

and accepts a hydrogen bond from another H_2O_2 molecule, along with its first coordination shell ($2H_2O_2{\cdot}3H_2O$). Since the crystal structure only identified the oxygen atom positions, hydrogen atoms were added to form the corresponding hydrogen bonds, as implicitly required by the crystal structure,[9] consistent with the following relationship between the hydrogen bond type and the $r_{O\cdots O}$ distance: $r_{O\cdots O} \sim 2.69$ Å for OOH···O, $r_{O\cdots O} \sim 2.74$ Å for OH···O, and $r_{O\cdots O} \sim 2.76$ Å for OH···OO, where O and OO pertain to water and H_2O_2, respectively.[9]

Density functional theory vibrational frequency calculations of the $H_2O_2{\cdot}4H_2O$ and $2H_2O_2{\cdot}3H_2O$ clusters were performed using the Perdew−Burke−Ernzerhof functional and 6-31+G-(2d,p) basis set as implemented in the GAMESS 2018 R1 suite of programs.[40] The hydrogen geometries of the $H_2O_2{\cdot}4H_2O$ and $2H_2O_2{\cdot}3H_2O$ clusters were optimized while keeping the oxygen atoms fixed to their locations in the experimental crystal structure. The resulting optimized structures were then used to calculate the corresponding local-mode O−H stretch frequencies using a partial Hessian vibrational analysis.[41] Thus, these local-mode frequencies pertain to clusters in which all atoms are held fixed except one hydrogen atom (and the calculations are repeated for each hydrogen in the cluster).

Classical MD simulations of 0.03 M TBA solution were performed using GROMACS[42] at a temperature of 20 °C and a pressure of 1 bar with 9900 water molecules and 5 TBA molecules,[43] modeled using TIP4P-2005 and OPLS-AA potentials, respectively. A 20 ns production run was performed after 5 ns of equilibration. Coordination numbers were obtained by counting the number of water molecules in the first hydration shell of TBA, defined as those within 6.3 Å of the central carbon of TBA (corresponding to the position of the first minimum in the radial distribution function of the water oxygen and the central carbon of TBA).

RESULTS AND DISCUSSION

Figure 2A shows the Raman spectra of water (dashed blue) and 0.5 M aqueous H_2O_2 (dotted purple) at 20 °C, along with the corresponding Raman-MCR SC component (solid purple) spectra pertaining to H_2O_2 and its hydration shell. The lower two panels in Figure 2 show expanded views of the OH bend and stretch band regions. The most striking feature of these results is the appearance of at least four sub-bands in the OH stretch spectrum of dilute H_2O_2, whose assignments are supported by comparisons with the solid H_2O_2 dihydrate.

Table 1 compares our calculated cluster local-mode O−H frequencies, ω_{OH}, with those previously measured in the deuterated dihydrate ($D_2O_2{\cdot}2D_2O$) with ∼5% hydrogen.[23] The good agreement between the calculated and experimental frequencies is consistent with the following order of hydrogen bond strengths: OOH···O > OH···O > OH···OO. Thus, the hydrogen bond donated from H_2O_2 to water (OOH···O, $r_{O\cdots O} \sim 2.69$ Å) is significantly stronger than that donated from water to H_2O_2 (OH···OO, $r_{O\cdots O} \sim 2.76$ Å), while the water−water hydrogen bond (OH···O, $r_{O\cdots O} \sim 2.74$ Å) is intermediate in strength and its bond length is slightly shorter than that of both hexagonal ice (OH···O, $r_{O\cdots O} \sim 2.76$ Å)[44] and solid H_2O_2 (OOH···OO, $r_{O\cdots O} \sim 2.76$ Å).[6] The Raman spectra of solid crystalline pure H_2O_2 and its dihydrate also contain a peak near 2800 cm^{-1}, assigned to the H_2O_2 bend overtone ($2\nu_6$) that is Fermi resonance coupled to the H_2O_2 OH stretch fundamental (ν_1).[13,23]

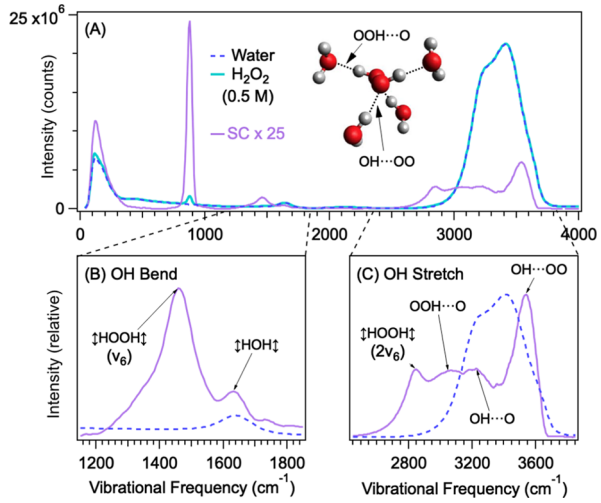

Figure 2. Raman and Raman-MCR spectra of 0.5 M aqueous H_2O_2. (A) Raw Raman spectra of water (dashed blue) and aqueous H_2O_2 solution (solid aqua) and the resulting Raman-MCR SC component spectrum pertaining to the dilute H_2O_2 molecule and its hydration shell (purple ×25). (B,C) Expanded views of the bend (B) and stretch (C) regions. The spectra in (C) are scaled so they have the same O−H areas, and the spectra in (B) are both multiplied by a factor of 4 relative to the spectra in (C).

Table 1. Calculated and Experimental Local-Mode O−H Vibrational Frequencies Pertaining to the Solid H_2O_2 Dihydrate and the Corresponding Clusters[a]

O−H stretch local mode	calculated		experimental	
	ω (cm^{-1})	$\Delta\omega$ (cm^{-1})	ω (cm^{-1})	$\Delta\omega$ (cm^{-1})
OOH···O	3083 [3046]	0	3121	0
OH···O	[3235]	152	3234	113
OH···OO	3376 [3375]	292	3385	264

[a]The calculated frequencies are obtained from either cluster (B) or (C, in square brackets) shown in Figure 1. The OH···O frequency pertains to that of the other hydrogen on the water molecule that donates a hydrogen bond to H_2O_2. The last two columns pertain to the experimental local-mode OH frequencies of the solid deuterated dihydrate ($D_2O_2{\cdot}2D_2O$) isotopically diluted with ∼5% H.[23] $\Delta\omega$ is the shift relative to the OOH···O band.

These dihydrate crystal results suggest that the four Raman-MCR SC sub-bands of H_2O_2 in liquid water may be assigned as indicated in Figure 2C. Specifically, the lowest frequency sub-band near 2850 cm^{-1} is assigned to the H_2O_2 bend overtone ($2\nu_6$);[13,23] the sub-band with the highest intensity and frequency (at ∼3540 cm^{-1}) is assigned to the relatively weak OH···OO hydrogen bonds from water to H_2O_2; and the two smaller sub-bands that peaked near ∼3065 and ∼3225 cm^{-1} are assigned to OOH···O and OH···O bonds, respectively. The ∼3225 cm^{-1} sub-band is likely due to the second OH group of the OH···OO water molecule (as further discussed below).

Figure 3 shows the Raman-MCR SC spectra obtained from aqueous H_2O_2 solutions with concentrations ranging from 1 to 9.8 M (∼30 wt %) at 20 °C. The colored curves in the upper two panels show the SC spectra in the OH bend (A) and stretch (B) spectral regions compared with the corresponding pure water (dashed blue) bands. Each of these H_2O_2 SC spectra was obtained from a pairwise SMCR analysis of the

https://doi.org/10.1021/acs.jpcb.1c03107
J. Phys. Chem. B 2021, 125, 6986−6993

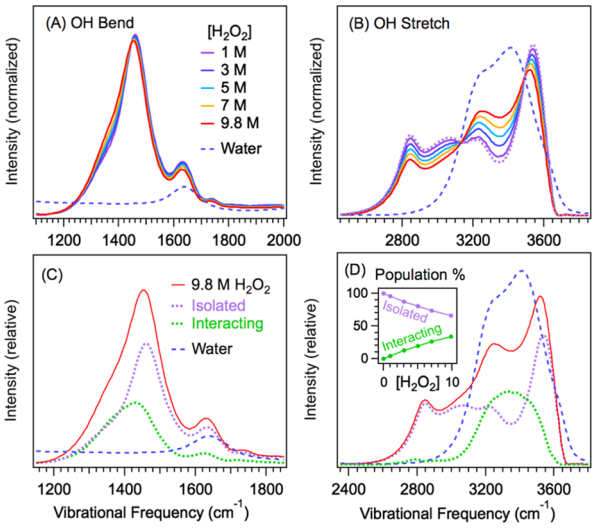

Figure 3. Concentration-dependent Raman-MCR SC spectra of aqueous H_2O_2. Panels (A,B) show the concentration-dependent SC spectra of H_2O_2 in the bend and stretch regions, including the SC spectrum extrapolated to zero concentration (dotted purple) as well as the corresponding pure water spectrum (dashed blue). Panels (C,D) show the results of a second-round SMCR decomposition of the spectra in Figure 2A,B into isolated (dotted purple) and interacting (dotted green) H_2O_2 component spectra. The spectra in (C,D) pertain to the 9.8 M solution, and the inset panel in (D) shows how the relative intensities of the isolated and interacting components depend on H_2O_2 concentration.

corresponding solution and pure water spectra. The approximate concentration independence of these concentration-normalized SC bend and stretch bands imply that they arise primarily from intramolecular vibrations of H_2O_2. However, the area of the SC OH stretch band is somewhat too large to be attributable to H_2O_2 alone, implying that some water molecules directly hydrogen-bonded to H_2O_2 are retained over this concentration range (as further discussed below and quantified in the Supporting Information).

Two additional lines of evidence suggest that the perturbed hydration-shell water molecules contribute to the SC spectra in Figure 3A,B. First of all, the bend side band near 1640 cm^{-1} is very close to the corresponding bend band of pure water (at ~1637 cm^{-1}), and no such peak appears in the Raman spectra of pure solid[13] and liquid[14] H_2O_2. Thus, we assign the 1640 cm^{-1} SC band to the bend vibrations of water molecules in the hydration shell of H_2O_2 whose frequency differs slightly from that of pure liquid water. The very small peak near 1740 cm^{-1} is likely an overtone of the anharmonic O−O stretch, which also appears in the pure H_2O_2 liquid Raman spectrum.[11,14] Additionally, the largest O−H stretch sub-band in Figure 2B, that peaked at ~3534 cm^{-1}, does not correlate with any peak in the Raman spectrum of pure liquid and solid H_2O_2 but is not far from a pair of peaks in the solid H_2O_2 dihydrate spectrum (at ~3380 and ~3416 cm^{-1}), assigned to relatively weak OH···OO hydrogen bonds between water and H_2O_2,[23] consistent with our assignment of the ~3534 cm^{-1} peak to water molecules that donate hydrogen bonds to H_2O_2 (whose higher frequency indicates a weaker hydrogen bond than in the H_2O_2 dihydrate).

Additional evidence confirming our assignments comes from the largest peak in Figure 3A, at ~1460 cm^{-1}, which is due to the H_2O_2 bend, as its frequency is close to the corresponding bend bands of pure liquid[11] and solid[13] H_2O_2. Thus, the lowest frequency band in Figure 3B near 2800 cm^{-1} is consistent with that of the bend overtone whose intensity is enhanced by Fermi resonance with a neighboring H_2O_2 OH stretch vibration of the same symmetry (as is also the case in solid H_2O_2).[13] Note that the sub-band that peaked at ~3065 cm^{-1} is sufficiently close to the bend overtone to produce significant Fermi resonance coupling and is consistent with its assignment to the very strong OOH···O hydrogen bond. Our assignment of the remaining SC sub-band near 3225 cm^{-1} to the other OH group of an OH···OO water molecule is consistent with its similar frequency to other water OH···O hydrogen-bonded OH groups. However, the assignment of this sub-band is complicated by the emergence of another band in this region at higher concentrations, as seen in Figure 3B. An important hint regarding these concentration-dependent spectral changes is provided by the nearly perfect isosbestic points at ~3130 and ~3490 cm^{-1} in the spectra in Figure 3B, suggesting that all these spectra arise from a linear combination of two spectral species whose relative intensities change with increasing concentration.

The significance of the isosbestic behavior of the SC spectra in the upper panels of Figure 3 is clarified by the second-round SMCR decomposition results shown in the lower two panels in Figure 3 (obtained as described in the Materials and Methods section). These results imply that all SC spectra in the upper panels of Figure 3 are representable as a linear combination of the dotted-purple and dotted-green component spectra shown in the lower panels. The inset in Figure 3D shows how the relative intensities of the two components change as a function of the H_2O_2 concentration. The fact that the intensity of the high concentration (interacting) component remains smaller than that of the isolated component even at 10 M concentration implies that H_2O_2 molecules have little propensity to aggregate with each other. Additional measurements at 5.0 °C indicate that the aggregation propensity increases slightly at lower temperature and is enthalpically favored (as further described in the Supporting Information, Section S1a and Figure S1).

The interacting H_2O_2 component (dotted-green spectrum) that emerges at high concentrations is quite similar to the previously reported Raman spectrum of pure liquid H_2O_2[11,14] as both have OH bend and stretch bands of about the same frequency and width. Moreover, the Raman spectrum of pure liquid H_2O_2 also has a very small bend overtone band near 2800 cm^{-1}, whose relative intensity is similar to that in the green curve in Figure 3D. The low intensity of the very small peak near 2800 cm^{-1} in the dotted green spectrum is consistent with its much weaker Fermi resonance with the corresponding H_2O_2 OH stretch band that peaked near 3350 cm^{-1}. Thus, the dotted-green spectrum in the lower panels of Figure 3 is evidently associated with interacting H_2O_2 molecules, and thus the bend peak near 1430 cm^{-1} and the broad stretch peak near 3350 cm^{-1} are assigned to H_2O_2 molecules that are hydrogen-bonded to other H_2O_2 molecules. The somewhat flat-toped shape of the broad 3350 cm^{-1} band may indicate that the interacting H_2O_2 OH stretch band is composed of overlapping sub-bands with different dihedral angles or hydrogen bond strengths.[11] Further support for the presence of a distribution of hydrated H_2O_2 structures is provided by our additional polarized Raman-MCR spectra (see Supporting Information Section S1b and Figure S3).

https://doi.org/10.1021/acs.jpcb.1c03107
J. Phys. Chem. B 2021, 125, 6986−6993

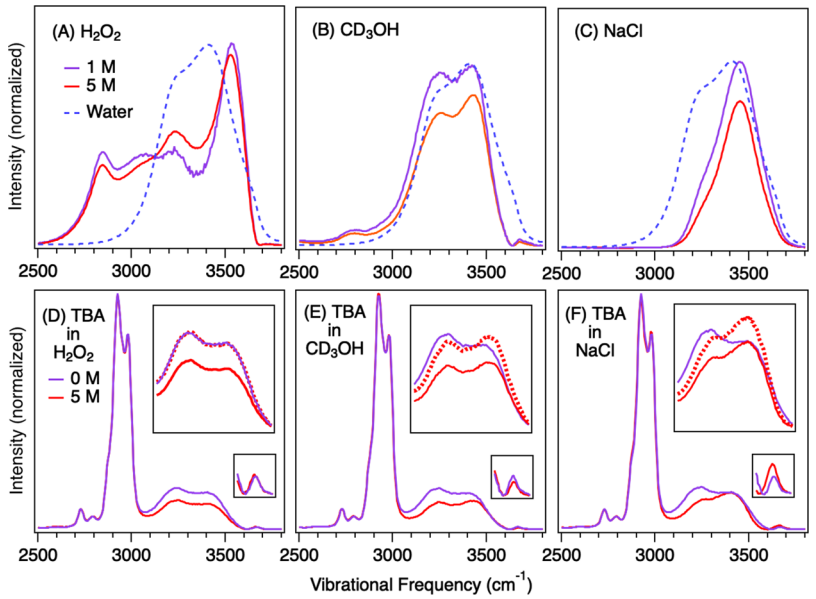

Figure 4. Comparison of the hydration-shell spectra of aqueous H_2O_2 (A), CD_3OH (B), and NaCl (C) at concentrations of 1 and 5 M (and water scaled to approximately the same peak height). The lower three panels (D−F) show the influence of the above three solutes on the hydration shell of 0.5 M TBA. The large inset panels in (D−F) show expanded views of the TBA hydration-shell hydrogen-bonded OH stretch bands, and the dotted red curves are the TBA SC spectra in the 5 M solutions scaled to the same area as the SC spectrum of TBA in water (with a 0 M solute concentration). The small inset panels in (D−F) show expanded views of the corresponding dangling OH bands.

We next describe the evidence leading to our conclusion that H_2O_2 perturbs the structure of water less than other solutes of comparable size by comparing the hydration-shell spectra of aqueous H_2O_2, CD_3OH, and NaCl, as well as the influence of these three solutes on the hydration-shell spectrum of TBA.

The top three panels in Figure 4 compare the Raman-MCR SC spectra of H_2O_2, CD_3OH, and NaCl (and pure water) in the O−H stretch region. Figure 4A reproduces the previously shown SC spectra of H_2O_2, whose nearly constant area implies that the only water molecules significantly perturbed by H_2O_2 are those that directly donate a hydrogen bond to H_2O_2 and are substantially retained over this concentration range (as further discussed in the Supporting Information, Section S1c). Figure 4B,C compares the quite different SC spectra of 1 and 5 M CD_3OH and NaCl, respectively. These normalized SC spectra arise primarily from the water molecules that are perturbed by the two solutes. The concentration-dependent decrease in the areas of these SC OH bands is consistent with the displacement of some hydration-shell water molecules by neighboring solute molecules. Although the shapes of these hydration-shell spectra appear to be nearly concentration-independent, close inspection reveals some shape changes, such as the slight decrease in the relative intensity of the 3200 cm^{-1} sub-band in the hydration shell of CD_3OH at higher concentration, consistent with a slight decrease in the tetrahedrality of the hydration shells of two neighboring CD_3OH solutes.[37,43]

More telling evidence of the exceptionally small influence of H_2O_2 on water structure is provided by the results shown in the lower three panels in Figure 4. The OH bands in these spectra (at frequencies >3000 cm^{-1}) reveal how 5 M aqueous H_2O_2, CD_3OH, and NaCl solutions influence the hydration shell of TBA (whose relatively low 0.5 M concentration assures minimal interactions between TBA molecules).[45] Figure 4D reveals that 5 M H_2O_2 decreases the hydration shell OH band area of TBA, with virtually no change in the shape of the band. This shape invariance is more clearly evident in the large inset panel in Figure 4D, in which the dotted red curve is the same as the solid red (5 M) SC spectrum scaled to the same area as the purple SC spectrum (in pure water). Thus, the essentially identical shapes of the dotted red and purple hydration-shell OH bands imply that adding 5 M H_2O_2 has little influence on the hydration-shell structure of TBA (other than the displacement of some water molecules by H_2O_2). Further evidence of the exceptionally small influence of H_2O_2 on the entire SC spectrum of TBA, including the bend band, is provided in the Supporting Information (Figure S2).

Our MD simulations (described in the Computational Methods section) indicate that the full first hydration shell of TBA contains ∼30 water molecules. This number may be combined with the observed decrease in the TBA hydration-shell OH stretch area to estimate the fraction of the TBA hydration-shell water molecules that are displaced by H_2O_2. Specifically, the ∼18% decrease in area in the SC OH stretch bands in Figure 4D indicates that ∼5 water molecules are displaced from the TBA hydration shell in 5 M H_2O_2. Since the partial molar volume of H_2O_2 is ∼30% larger than that of water,[4] this implies that there are ∼4 H_2O_2 molecules in the hydration shell of TBA dissolved in 5 M H_2O_2, which is about the number expected if the local concentration of H_2O_2 were the same as its bulk concentration. But, again, these H_2O_2 molecules in the hydration shell of TBA do not significantly change the structure of the remaining hydration-shell water molecules.

Figure 4E,F shows the corresponding results pertaining to TBA dissolved in pure water and 5 M aqueous solutions of either CD_3OH or NaCl, respectively. These solutes are found to change both the area and shape of the TBA hydration-shell spectra. The decrease in area of the hydration-shell OH bands in Figure 4E,F is again consistent with the displacement of water from the hydration shell of TBA. But, unlike the H_2O_2 solutions, CD_3OH and NaCl solutions significantly change the

https://doi.org/10.1021/acs.jpcb.1c03107
J. Phys. Chem. B 2021, 125, 6986−6993

shape of the TBA hydration-shell OH band, as is most clearly evident when comparing the purple and dashed-red hydration-shell bands (both of which are again scaled to the same area). Note that both CD_3OH and NaCl induce a decrease in the relative intensity of the 3200 cm^{-1} sub-band in the hydration shell of TBA. Such a decrease in the 3200 cm^{-1} sub-band intensity is consistent with a decrease in the tetrahedral order of the TBA hydration shell[43,46] (as further described in the Supporting Information).

The small inset panels in Figure 4D−F show the corresponding water dangling OH bands in the hydration shell of TBA.[47,48] Note that the dangling OH band in the SC spectrum of TBA is essentially unchanged with increasing H_2O_2 concentration. However, both CD_3OH and NaCl significantly change the dangling OH band area but in opposite directions. Given that these dangling OH groups arise primarily from water molecules that are in direct contact with TBA,[49] their insensitivity to H_2O_2 implies that 5 M H_2O_2 does not disrupt those OH groups, even though H_2O_2 displaces some of the other hydrogen-bonded water molecules in the hydration shell of TBA. In contrast, the decrease in the TBA dangling OH band area with increasing CD_3OH concentration implies that CD_3OH displaces some of the very close water molecules as it comes into direct contact with TBA. On the other hand, the increase in the dangling OH band area with increasing NaCl concentration implies that Na^+ and/or Cl^- ions disrupt the TBA hydration-shell structure sufficiently to significantly increase the population of dangling OH groups.

CONCLUSIONS AND IMPLICATIONS

Our Raman-MCR spectra of aqueous H_2O_2 provide the first measurements of the Raman spectra of dilute H_2O_2 and its hydration-shell, whose four sub-bands are assigned with the aid of prior solid dihydrate spectral measurements and our own vibrational frequency calculations. Our results also provide quantitative evidence of the exceptionally small influence of H_2O_2 on the water structure when compared to other solutes of comparable size (CD_3OH and NaCl), as most clearly revealed by comparisons of the hydration-shell spectra of TBA dissolved in 5 M aqueous solutions H_2O_2, CD_3OH, and NaCl.

The minimal influence of H_2O_2 on the water structure, combined with the more facile supercooling of aqueous H_2O_2 solutions, suggests that such solutions may be useful for future studies pertaining to the possible existence of a liquid−liquid phase transition in supercooled water[25−27] as well as a low-temperature hydration-shell structural crossover,[50,51] both of which may have biological[50−53] and atmospheric[54−56] implications. However, open questions remain regarding the similarity between the structure of supercooled water and aqueous H_2O_2, given that some of the density, compressibility, and heat capacity anomalies of supercooled water are suppressed in aqueous H_2O_2.[17,25,57]

ASSOCIATED CONTENT

Supporting Information

The Supporting Information is available free of charge at https://pubs.acs.org/doi/10.1021/acs.jpcb.1c03107.

Aqueous H_2O_2 Raman cross section, polarized Raman spectra, hydration-shell tetrahedrality, and isosbestic behavior (PDF)

AUTHOR INFORMATION

Corresponding Author

Dor Ben-Amotz − *Department of Chemistry, Purdue University, West Lafayette, Indiana 47907, United States;* orcid.org/0000-0003-4683-5401; Email: bendor@purdue.edu

Authors

Aria J. Bredt − *Department of Chemistry, Purdue University, West Lafayette, Indiana 47907, United States*

Denilson Mendes de Oliveira − *Department of Chemistry, Purdue University, West Lafayette, Indiana 47907, United States;* orcid.org/0000-0002-2579-8405

Andres S. Urbina − *Department of Chemistry, Purdue University, West Lafayette, Indiana 47907, United States;* orcid.org/0000-0001-6482-4736

Lyudmila V. Slipchenko − *Department of Chemistry, Purdue University, West Lafayette, Indiana 47907, United States;* orcid.org/0000-0002-0445-2990

Complete contact information is available at: https://pubs.acs.org/10.1021/acs.jpcb.1c03107

Author Contributions

A.J.B. and D.M.d.O. contributed equally. The manuscript was written jointly by all authors. The experiments were performed by A.J.B. and D.M.d.O. The vibrational frequency and MD calculations were performed by A.S.U. The work was conceived and directed by D.B.-A. and L.V.S.

Notes

The authors declare no competing financial interest.

ACKNOWLEDGMENTS

We acknowledge support by the National Science Foundation (grant number CHE-1763581). We thank Prof. Nicolas Giovambattista for suggesting that aqueous hydrogen peroxide would be an interesting system to investigate using Raman-MCR (with possible supercooled water implications), Dr. Matthias Zeller for help in locating and interpreting previously published crystal structures, and Emily M. Cataldo for performing some preliminary Raman measurements of aqueous H_2O_2 as an undergraduate research assistant.

REFERENCES

(1) Maass, O.; Herzberg, O. W. The Properties of Pure Hydrogen Peroxide II. *J. Am. Chem. Soc.* **1920**, *42*, 2569−2570.

(2) Foley, W. T.; Giguère, P. A. Hydrogen Peroxide and Its Analogues. 2. Phase Equilibrium in the System Hydrogen Peroxide Water. *Can. J. Chem.* **1951**, *29*, 123−132.

(3) Scatchard, G.; Kavanagh, G. M.; Ticknor, L. B. Vapor Liquid Equilibrium. 8. Hydrogen Peroxide Water Mixtures. *J. Am. Chem. Soc.* **1952**, *74*, 3715−3720.

(4) Mitchell, A. G.; Wynne-Jones, W. F. K. Thermodynamic and Other Properties of Solutions Involving Hydrogen Bonding. *Discuss. Faraday Soc.* **1953**, *15*, 161−168.

(5) Baraban, J. H.; Changala, P. B.; Stanton, J. F. The Equilibrium Structure of Hydrogen Peroxide. *J. Mol. Spectrosc.* **2018**, *343*, 92−95.

(6) Savariault, J. M.; Lehmann, M. S. Experimental Determination of the Deformation Electron-Density in Hydrogen-Peroxide by Combination of X-Ray and Neutron-Diffraction Measurements. *J. Am. Chem. Soc.* **1980**, *102*, 1298−1303.

(7) Busing, W. R.; Levy, H. A. Crystal and Molecular Structure of Hydrogen Peroxide - a Neutron-Diffraction Study. *J. Chem. Phys.* **1965**, *42*, 3054−3059.

(8) Abrahams, S. C.; Collin, R. L.; Lipscomb, W. N. The Crystal Structure of Hydrogen Peroxide. *Acta Crystallogr.* **1951**, *4*, 15−20.
(9) Olovsson, I.; Templeton, D. H.; Rundqvist, S.; Varde, E.; Westin, G. The Crystal Structure of Hydrogen Peroxide Dihydrate. *Acta Chem. Scand.* **1960**, *14*, 1325−1332.
(10) Chernyshov, I. Y.; Vener, M. V.; Prikhodchenko, P. V.; Medvedev, A. G.; Lev, O.; Churakov, A. V. Peroxosolvates: Formation Criteria, H_2O_2 Hydrogen Bonding, and Isomorphism with the Corresponding Hydrates. *Cryst. Growth Des.* **2017**, *17*, 214−220.
(11) Giguère, P. A.; Chen, H. Hydrogen-Bonding in Hydrogen-Peroxide and Water - a Raman-Study of the Liquid-State. *J. Raman Spectrosc.* **1984**, *15*, 199−204.
(12) Giguére, P. A.; Srinivasan, T. K. K. A Raman Study of H_2O_2 and D_2O_2 Vapor. *J. Raman Spectrosc.* **1974**, *2*, 125−132.
(13) Arnau, J. L.; Giguère, P. A.; Abe, M.; Taylor, R. C. Vibrational Spectra and Normal Coordinate Analysis of Crystalline H_2O_2, D_2O_2 and HDO_2. *Spectrochim. Acta, Part A* **1974**, *30*, 777−796.
(14) Taylor, R. C.; Cross, P. C. Raman Spectra of Hydrogen Peroxide in Condensed Phases. 1. Spectra of the Pure Liquid and Its Aqueous Solutions. *J. Chem. Phys.* **1956**, *24*, 41−44.
(15) Gross, P. M.; Taylor, R. C. The Dielectric Constants of Water, Hydrogen Peroxide and Hydrogen Peroxide-Water Mixtures. *J. Am. Chem. Soc.* **1950**, *72*, 2075−2080.
(16) Lyashchenko, A. K.; Goncharov, V. S.; Yastremskii, P. S. Structure and Dielectric Properties of Aqueous Solutions of Hydrogen-Peroxide. *J. Struct. Chem.* **1976**, *17*, 871−876.
(17) Minoguchi, A.; Richert, R.; Angell, C. A. Dielectric Relaxation in Aqueous Solutions of Hydrazine and Hydrogen Peroxide: Water Structure Implications. *J. Phys. Chem. B* **2004**, *108*, 19825−19830.
(18) Thürmer, S.; Seidel, R.; Winter, B.; Ončák, M.; Slavíček, P. Flexible H_2O_2 in Water: Electronic Structure from Photoelectron Spectroscopy and Ab Initio Calculations. *J. Phys. Chem. A* **2011**, *115*, 6239−6249.
(19) Biswas, A.; Mallik, B. S. Conformational Dynamics of Aqueous Hydrogen Peroxide from First Principles Molecular Dynamics Simulations. *Phys. Chem. Chem. Phys.* **2020**, *22*, 28286−28296.
(20) Moin, S. T.; Hofer, T. S.; Randolf, B. R.; Rode, B. M. An Ab Initio Quantum Mechanical Charge Field Molecular Dynamics Simulation of Hydrogen Peroxide in Water. *Comput. Theor. Chem.* **2012**, *980*, 15−22.
(21) Yu, C.-Y.; Yang, Z.-Z. A Systemic Investigation of Hydrogen Peroxide Clusters $(H_2O_2)(N)$ (N=1-6) and Liquid-State Hydrogen Peroxide: Based on Atom-Bond Electronegativity Equalization Method Fused into Molecular Mechanics and Molecular Dynamics. *J. Phys. Chem. A* **2011**, *115*, 2615−2626.
(22) Kulkarni, A. D.; Pathak, R. K.; Bartolotti, L. J. Structures, Energetics, and Vibrational Spectra of H_2O_2...$(H_2O)(N)$, N=1-6 Clusters: Ab Initio Quantum Chemical Investigations. *J. Phys. Chem. A* **2005**, *109*, 4583−4590.
(23) Arnau, J. L.; Giguere, P. A. Spectroscopic Study on Hydrogen-Peroxide Derivatives. 6. Dihydrated H_2O_2-$2H_2O$. *Can. J. Spectrosc.* **1972**, *17*, 121−124.
(24) Giguère, P. A.; Harvey, K. B. An Infrared Study of Hydrogen Bonding in Solid H_2O_2 and H_2O-H_2O_2 Mixtures. *J. Mol. Spectrosc.* **1959**, *3*, 36−45.
(25) Woutersen, S.; Ensing, B.; Hilbers, M.; Zhao, Z.; Angell, C. A. A Liquid-Liquid Transition in Supercooled Aqueous Solution Related to the HDA-LDA Transition. *Science* **2018**, *359*, 1127−1131.
(26) Gallo, P.; Loerting, T.; Sciortino, F. Supercooled Water: A Polymorphic Liquid with a Cornucopia of Behaviors. *J. Chem. Phys.* **2019**, *151*, 210401.
(27) Sellberg, J. A.; Huang, C.; McQueen, T. A.; Loh, N. D.; Laksmono, H.; Schlesinger, D.; Sierra, R. G.; Nordlund, D.; Hampton, C. Y.; Starodub, D.; et al. Ultrafast X-Ray Probing of Water Structure Below the Homogeneous Ice Nucleation Temperature. *Nature* **2014**, *510*, 381−384.
(28) Lee, J. K.; Han, H. S.; Chaikasetsin, S.; Marron, D. P.; Waymouth, R. M.; Prinz, F. B.; Zare, R. N. Condensing Water Vapor to Droplets Generates Hydrogen Peroxide. *Proc. Natl. Acad. Sci. U.S.A.* **2020**, *117*, 30934−30941.
(29) Wang, Y.; Li, F.; Fang, W.; Sun, C.; Men, Z. H_2O_2-Induced Hydrogen Bond Water Networks Enhanced on Stimulated Raman Scattering. *J. Raman Spectrosc.* **2019**, *50*, 1890−1895.
(30) Ju, X.-H.; Xiao, J.-J.; Xiao, H.-M. Theoretical Study on Intermolecular Interactions and Thermodynamic Properties of Water-Hydrogen Peroxide Clusters. *J. Mol. Struct.: THEOCHEM* **2003**, *626*, 231−238.
(31) González, L.; Mo, O.; Yanez, M. High-Level Ab Initio Versus DFT Calculations on $(H_2O_2)_2$ and H_2O_2-H_2O Complexes as Prototypes of Multiple Hydrogen Bond Systems. *J. Comput. Chem.* **1997**, *18*, 1124−1135.
(32) Martins-Costa, M. T. C.; Ruiz-López, M. F. Molecular Dynamics of Hydrogen Peroxide in Liquid Water Using a Combined Quantum/Classical Force Field. *Chem. Phys.* **2007**, *332*, 341−347.
(33) Gierszal, K. P.; Davis, J. G.; Hands, M. D.; Wilcox, D. S.; Slipchenko, L. V.; Ben-Amotz, D. Π-Hydrogen Bonding in Liquid Water. *J. Phys. Chem. Lett.* **2011**, *2*, 2930−2933.
(34) Matt, S. M.; Ben-Amotz, D. Influence of Intermolecular Coupling on the Vibrational Spectrum of Water. *J. Phys. Chem. B* **2018**, *122*, 5375−5380.
(35) Lawton, W. H.; Sylvestre, E. A. Self Modeling Curve Resolution. *Technometrics* **1971**, *13*, 617−633.
(36) Perera, P.; Wyche, M.; Loethen, Y.; Ben-Amotz, D. Solute-Induced Perturbations of Solvent-Shell Molecules Observed Using Multivariate Raman Curve Resolution. *J. Am. Chem. Soc.* **2008**, *130*, 4576−4577.
(37) Davis, J. G.; Gierszal, K. P.; Wang, P.; Ben-Amotz, D. Water Structural Transformation at Molecular Hydrophobic Interfaces. *Nature* **2012**, *491*, 582−585.
(38) Zhang, D.; Ben-Amotz, D. Enhanced Chemical Classification of Raman Images in the Presence of Strong Fluorescence Interference. *Appl. Spectrosc.* **2000**, *54*, 1379−1383.
(39) Savitzky, A.; Golay, M. J. E. Smoothing and Differentiation of Data by Simplified Least Squares Procedures. *Anal. Chem.* **1964**, *36*, 1627−1639.
(40) Barca, G. M. J.; Bertoni, C.; Carrington, L.; Datta, D.; De Silva, N.; Deustua, J. E.; Fedorov, D. G.; Gour, J. R.; Gunina, A. O.; Guidez, E.; et al. Recent Developments in the General Atomic and Molecular Electronic Structure System. *J. Chem. Phys.* **2020**, *152*, 154102.
(41) Li, H.; Jensen, J. H. Partial Hessian Vibrational Analysis: The Localization of the Molecular Vibrational Energy and Entropy. *Theor. Chem. Acc.* **2002**, *107*, 211−219.
(42) Abraham, M. J.; Murtola, T.; Schulz, R.; Páll, S.; Smith, J. C.; Hess, B.; Lindahl, E. Gromacs: High Performance Molecular Simulations through Multi-Level Parallelism Laptops to Supercomputers. *SoftwareX* **2015**, *1−2*, 19−25.
(43) Wu, X.; Lu, W.; Streacker, L. M.; Ashbaugh, H. S.; Ben-Amotz, D. Temperature-Dependent Hydrophobic Crossover Length Scale and Water Tetrahedral Order. *J. Phys. Chem. Lett.* **2018**, *9*, 1012−1017.
(44) Bergmann, U.; Di Cicco, A.; Wernet, P.; Principi, E.; Glatzel, P.; Nilsson, A. Nearest-Neighbor Oxygen Distances in Liquid Water and Ice Observed by X-Ray Raman Based Extended X-Ray Absorption Fine Structure. *J. Chem. Phys.* **2007**, *127*, 174504.
(45) Rankin, B. M.; Ben-Amotz, D.; van der Post, S. T.; Bakker, H. J. Contacts between Alcohols in Water Are Random Rather Than Hydrophobic. *J. Phys. Chem. Lett.* **2015**, *6*, 688−692.
(46) Morawietz, T.; Marsalek, O.; Pattenaude, S. R.; Streacker, L. M.; Ben-Amotz, D.; Markland, T. E. The Interplay of Structure and Dynamics in the Raman Spectrum of Liquid Water over the Full Frequency and Temperature Range. *J. Phys. Chem. Lett.* **2018**, *9*, 851−857.
(47) Davis, J. G.; Rankin, B. M.; Gierszal, K. P.; Ben-Amotz, D. On the Cooperative Formation of Non-Hydrogen Bonded Water at Molecular Hydrophobic Interfaces. *Nat. Chem.* **2013**, *5*, 796−802.
(48) Perera, P. N.; Fega, K. R.; Lawrence, C.; Sundstrom, E. J.; Tomlinson-Phillips, J.; Ben-Amotz, D. Observation of Water Dangling

https://doi.org/10.1021/acs.jpcb.1c03107
J. Phys. Chem. B 2021, 125, 6986−6993

OH Bonds around Dissolved Nonpolar Groups. *Proc. Natl. Acad. Sci. U.S.A.* **2009**, *106*, 12230−12234.
(49) Tomlinson-Phillips, J.; Davis, J.; Ben-Amotz, D.; Spångberg, D.; Pejov, L.; Hermansson, K. Structure and Dynamics of Water Dangling OH Bonds in Hydrophobic Hydration Shells. Comparison of Simulation and Experiment. *J. Phys. Chem. A* **2011**, *115*, 6177−6183.
(50) Qvist, J.; Halle, B. Thermal Signature of Hydrophobic Hydration Dynamics. *J. Am. Chem. Soc.* **2008**, *130*, 10345−10353.
(51) Duboué-Dijon, E.; Fogarty, A. C.; Laage, D. Temperature Dependence of Hydrophobic Hydration Dynamics: From Retardation to Acceleration. *J. Phys. Chem. B* **2014**, *118*, 1574−1583.
(52) Eickhoff, L.; Dreischmeier, K.; Zipori, A.; Sirotinskaya, V.; Adar, C.; Reicher, N.; Braslavsky, I.; Rudich, Y.; Koop, T. Contrasting Behavior of Antifreeze Proteins: Ice Growth Inhibitors and Ice Nucleation Promoters. *J. Phys. Chem. Lett.* **2019**, *10*, 966−972.
(53) Lv, J.; Song, Y.; Jiang, L.; Wang, J. Bio-Inspired Strategies for Anti-Icing. *ACS Nano* **2014**, *8*, 3152−3169.
(54) Koop, T.; Luo, B.; Tsias, A.; Peter, T. Water Activity as the Determinant for Homogeneous Ice Nucleation in Aqueous Solutions. *Nature* **2000**, *406*, 611−614.
(55) Kreder, M. J.; Alvarenga, J.; Kim, P.; Aizenberg, J. Design of Anti-Icing Surfaces: Smooth, Textured or Slippery? *Nat. Rev. Mater.* **2016**, *1*, 15003.
(56) Murray, B. J.; O'Sullivan, D.; Atkinson, J. D.; Webb, M. E. Ice Nucleation by Particles Immersed in Supercooled Cloud Droplets. *Chem. Soc. Rev.* **2012**, *41*, 6519−6554.
(57) Oguni, M.; Angell, C. A. Heat-Capacities of H_2O+H_2O_2, and H_2O+N_2H_4, Binary-Solutions - Isolation of a Singular Component for Cp of Supercooled Water. *J. Chem. Phys.* **1980**, *73*, 1948−1954.

https://doi.org/10.1021/acs.jpcb.1c03107
J. Phys. Chem. B 2021, 125, 6986−6993